Electronic Supplementary Material (ESI) for Chemical Communications.

Supporting Information

In situ FTIR Study of CO_2 Reduction on Inorganic Analogues of Carbon Monoxide Dehydrogenase

Ji-Eun Lee,[a] Akira Yamaguchi,[a,b] Hideshi Ooka,[a] Tomohiro Kazami,[b] Masahiro Miyauchi,[b] Norio Kitadai,[c,d] and Ryuhei Nakamura*[a,c]

a Biofunctional Catalyst Research Team, RIKEN Center for Sustainable Resource Science, 2-1 Hirosawa, Wako, Saitama 351-0198, Japan.
E-mail: ryuhei.nakamura@riken.jp

b Department of Materials Science and Engineering, Tokyo Institute of Technology, 2-12-1 Ookayama, Meguro-ku, Tokyo 152-8552, Japan.

c Earth-Life Science Institute (ELSI), Tokyo Institute of Technology, 2-12-1 Ookayama, Meguro-ku, Tokyo 152-8550, Japan.

d Super-cutting-edge Grand and Advanced Research (SUGAR) Program, Institute for Extra-cutting-edge Science and Technology Avant-garde Research (X-star), Japan Agency for Marine-Earth Science and Technology (JAMSTEC), 2-15 Natsushima-cho, Yokosuka 237-0061, Japan.

Experimental Procedures

Materials

Graphite, aniline, nickel (II) acetate tetrahydrate ($Ni(OCOCH_3)_2{\cdot}4H_2O$), iron (II) chloride tetrahydrate ($FeCl_2{\cdot}4H_2O$), L-cysteine, deuterium oxide (D_2O), and potassium bicarbonate ($KHCO_3$) were purchased from Sigma-Aldrich. Oleylamine, sodium dodecyl sulfate (SDS), and ammonium persulfate (APS) were purchased from FUJIFILM Wako Pure Chemical Corporation. Nickel (II) chloride hexahydrate ($NiCl_2{\cdot}6H_2O$) and acetone were purchased from Kanto Chemical Co. Inc. Sodium di-n-butyldithiocarbamate ($NaS_2NC^iBu_2$, ca 45% in water) and tetraethylthiuram disulfide ($(Et_2NCS_2)_2$) were obtained from abcr GmbH and Tokyo Chemical Industry Co. Ltd., respectively.

Synthesis of Fe_3S_4 and $FeNi_2S_4$

The synthesis of greigite (Fe_2S_4) and violarite ($FeNi_2S_4$) samples was conducted by the slightly modified method reported by Roldan et al. (A. Roldan *et al.*, *Chem. Commun.* **2015**, *51*, 7501). For the greigite synthesis, 15.159 g of $NaS_2NC^iBu_2$ aq. mixed with 51 mL of water was dropped into 50 mL of 0.2 M $FeCl_3$ aq. over 10 min and stirred vigorously for 2 h. A precursor ($Fe(S_2CN^iBu_2)_3$) was obtained by centrifuge, followed by washing with 30 mL x 3 water and vacuum drying. 1 mmol of the precursor and 2 mmol of $(Et_2NCS_2)_2$ were dissolved into 100 mL of oleylamine and stirred for 1 h at 230 °C under N_2 atmosphere using a round-bottomed flask equipped with a condenser. The mixture was cooled down to room temperature naturally, and the resulted powder was obtained by centrifuge, followed by washing with 30 mL x 5 acetone and vacuum drying. Violarite was prepared by the identical procedure except for replacing $FeCl_3$ to the mixture of $FeCl_3$ and $NiCl_2$ with the molar ratio of 1:2.

Synthesis of NiFe-PANI nanoarchitectures

Graphene oxide (GO) was synthesized from graphite by a modified Hummers method. For synthesizing the binary substrate, the polymerization of aniline on the GO surface was performed by surfactant-assisted chemical oxidative polymerization. First, a well-dispersed GO solution (0.5 mg/mL) was prepared using 100 mL DI water. A total of 0.6 mL aniline monomer and 20 mg SDS were added to the 100 mL DI water and resulting solution was then mixed followed by an ultrasonication treatment for 15 min to yield a homogenous suspension. A total of 1.4 g APS in 50 mL of HCl (1 M) was then slowly added to the suspension and the resulting solution was stirred for 12 h at 0 °C to generate a green suspension of PANI-GO, which was then washed several times with DI water to remove residues of surfactant and monomer by centrifugation. Nanoparticles of NiFeS-PANI were synthesized by hydrothermal treatment in aqueous solutions. Briefly, the metal precursors of 0.3 mmol $Ni(acetate)_2{\cdot}H_2O$, 0.9 mmol $FeCl_2{\cdot}H_2O$, and 1.2 mmol L-cysteine were dissolved in 5 mL DI water. The solutions were mixed with 10 mL PANI-GO under stirring for 20 min and were then fabricated in a Teflon-lined, 100 mL auto-clave reaction vessel. After heating at 230◦C for 12 h, the reaction vessel was cooled to room temperature in air. The reference samples of PANI-rGO were also synthesized by the same procedural with NiFeS-PANI.

Electrochemical Measurements

Prior to the electrocatalytic evaluation, the catalysts (5 mg) dispersed in water (150 µL) were mixed with isopropyl alcohol (350 µL) and Nafion solution (50 µL, 5 wt.%, Aldrich). The catalyst ink was ultrasonicated for 30 min and drop-casted (100 µL) onto a carbon paper (1.5 x 1.5 cm^2) electrode. Electrocatalytic performance was assessed using a potentiostat in a three-electrode system consisting of silver chloride (Ag/AgCl, in saturated KCl) and platinum wire as the reference and counter electrodes, respectively, and 0.1 M $KHCO_3$ as the electrolyte. The overall potential was converted to the reversible hydrogen electrode (RHE) according to the equation E (versus RHE) = E (versus Ag/AgCl) + 0.197 + (0.0591 x pH). To evaluate the CO_2 reduction reaction (CO_2RR), electrochemical measurements were performed in an H-type electrochemical cell, and a Nafion membrane was used to separate the catholyte and the anolyte. The 0.1 M $KHCO_3$ electrolyte solution was purged with 20 sccm high-purity CO_2 gas for at least 1 h until saturated (pH 6.8).

The CO_2RR activity was measured by chronoamperometry at several fixed potentials, and the gaseous products CO, CH_4 and C_2H_6 were quantified using a gas chromatograph-mass spectrometry system (Shimadzu GCMS-QP2010) equipped with a capillary column (Micropacked-ST 3.0 m). Ultrahigh purity helium (He, 99.9999%) was used as a carrier gas. For the detection and quantification of H_2, a gas chromatograph (Shimadzu GC-8A) equipped with a thermal conductivity detector (TCD, C-R8A) was used with and argon (Ar, 99.999%) as a carrier gas. Liquid products were also analyzed by high-performance liquid chromatography (HPLC) and nuclear magnetic resonance (NMR) spectroscopy. The HPLC system (Shimadzu Prominence UFLC) was equipped with an inertSustain Amide column (5 µm, 4.6 x 150 mm, GL Sciences), auto-sampler, and UV-vis detector using 10 µL injection volumes. The retention time was 20 min at a flow rate of 0.2 mL min^{-1} and 40 °C. Calibration (R_2 > 0.9999) was conducted using standard concentrations of formate between 0.1 ~ 100 mM. ^1H NMR measurements were conducted with a JEOL ECA600 spectrometer (600 MHz) at the sample temperature of 25 °C. Typically, 0.5 mL of sample solution was mixed with 0.1 mL of D_2O (99.9 atom % D; Sigma-Aldrich) containing 1 mM DMSO (99.9 % D; Cambridge Isotope Laboratories, Inc.) and was placed in an NMR tube (5 mm outside diameter; Wako Pure Chemical Industries, Ltd.). DMSO-d_6 was used for the calibration of the 0-ppm position and to estimate the product and reactant concentrations as an internal standard. All experiment was performed at room temperature (25 °C).

***In situ* Attenuated total reflectance-Fourier-transform infrared (ATR FT-IR) spectroscopy**

In situ ATR FT-IR measurements were performed with a Bruker Vertex 60 equipped with a liquid nitrogen-cooled MCT detector and an ATR accessory. For the *in situ* technique, a sealed electrochemical cell with Pt as the counter electrode, electrocatalysts as the working electrode, and Ag/AgCl (in saturated KCl electrolyte) as the reference electrode was mounted in the spectrometer. The *in situ* ATR FT-IR measurements were obtained over a range of 4000 to 600 cm^{-1} by averaging 512 scans at a resolution of 4 cm^{-1}. The IR spectra were collected during chronoamperometry measurements from 0.4 to –1.0 V in Ar- or CO_2-saturated 0.1 M $KHCO_3$ and 0.1 M $KDCO_3$ electrolytes at different potentials. The reference spectrum was obtained at +0.4 V versus RHE.

Characterization and Methods

The synthesized metal sulfide nanostructures were observed by JEOL-7800F scanning electron microscopy (SEM). Transmission electron microscopy (TEM) images were acquired using a JEOL-JEM-2100F/SP operated at 200 kV. X-ray diffraction (XRD) patterns of all samples were recorded using an XRD spectrometer (SmartLab, Rigaku) with Cu Kα radiation (λ = 1.54059 Å) operated at 45 kV and 200 mA. Electrochemical analysis was performed on an HZ−5000 (Hokuto−Denko) potentiostat.

Results and Discussion

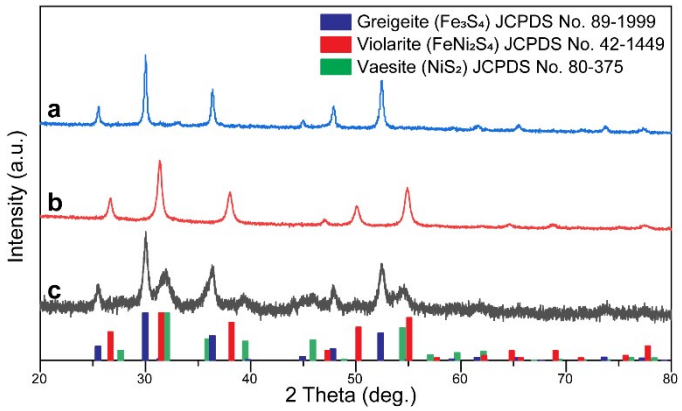

Figure S1. XRD patterns of (a) Fe_3S_4, (b) $FeNi_2S_4$, and (c) NiFeS-PANI samples.

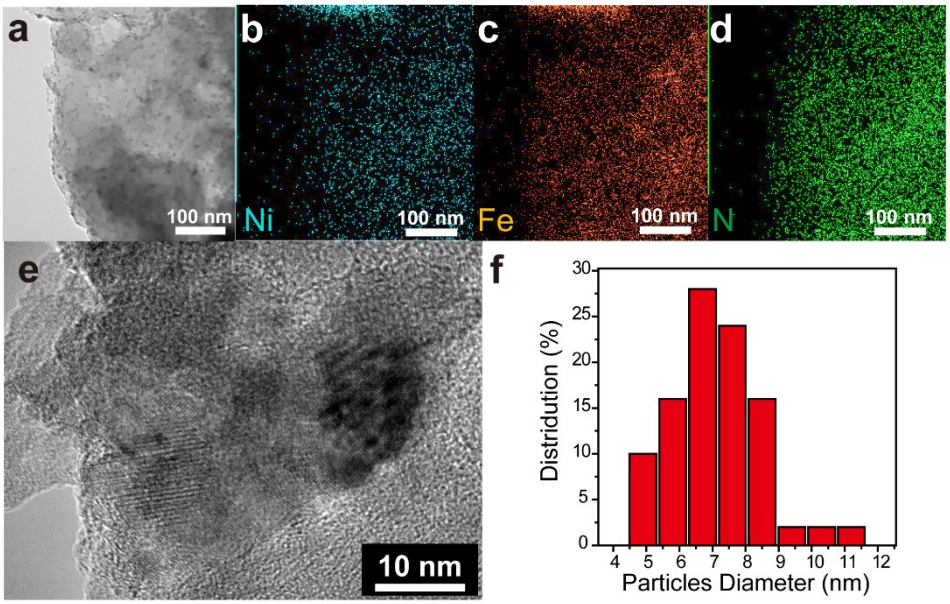

Figure S2. (a) TEM image of the NiFeS-PANI. (b)-(d) Images show elemental distribution on the surface of the NiFeS-PANI measured by TEM-EDS mapping of Ni, Fe, and S. (e) HR-TEM image of the NiFeS-PANI. (f) Histogram of particle size distribution obtained from the TEM images.

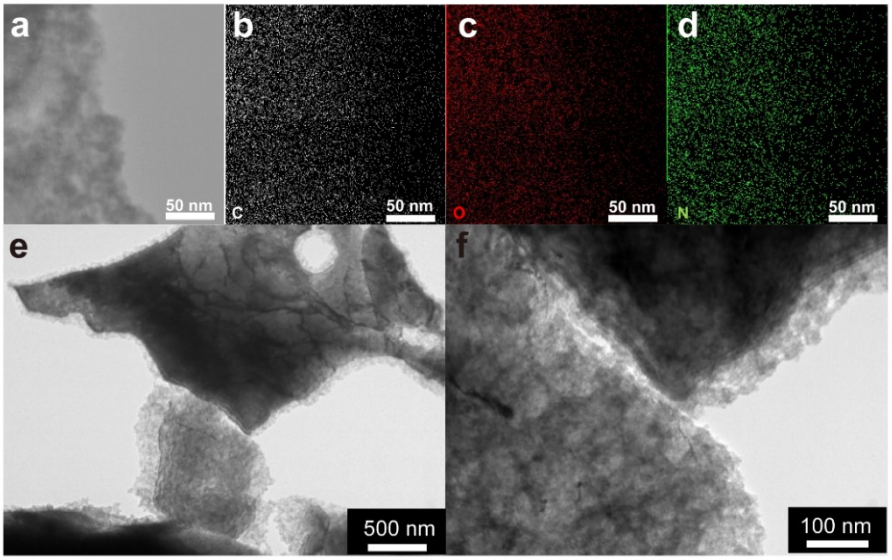

Figure S3. (a-b) TEM images of PANI-rGO. (c)-(f) Images show elemental distribution on the surface of PANI-rGO measured by TEM-EDS mapping of C, O and N.

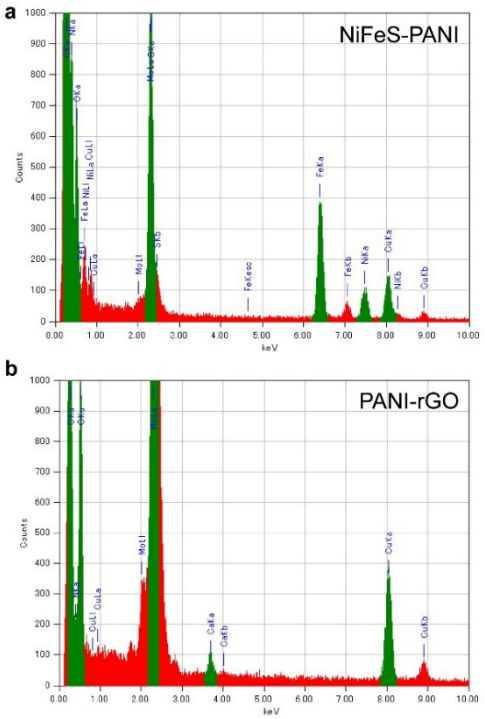

Figure S4. TEM-EDX spectra of (a) NIFeS-PANI and (b) PANI-rGO. The TEM-EDX analysis was conducted onto the Mo grid without carbon and Cu. The Cu signals in the background were originated from a TEM holder with a Cu retainer plater.

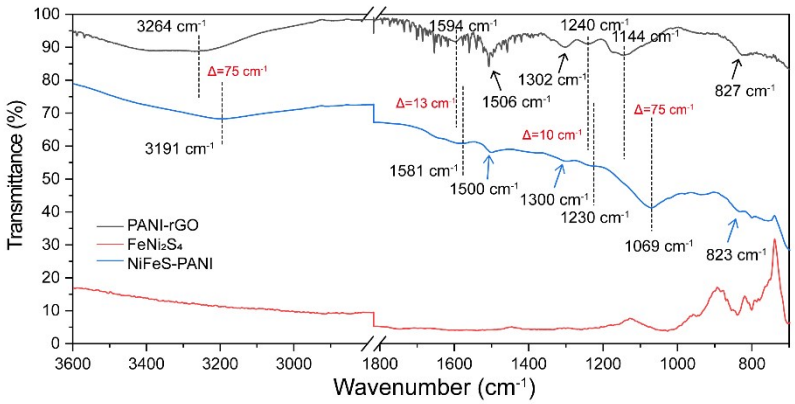

Figure S5. FT-IR spectra of PANI-rGO, $FeNi_2S_4$, and NiFeS-PANI nanostructures. The N-H stretching is distinctly shifted from 3264 cm^{-1} to 3191 cm^{-1}.The peaks of the quinonoid ring with a C-N stretching and a quinonoid unit of doped PANI are also shifted from 1144 to 1069 cm^{-1} and 1594 to 1581 cm^{-1}, respectively, upon the formation of the nanoparticles, indicating the weak electrostatic interaction of NiFeS with polyaniline.

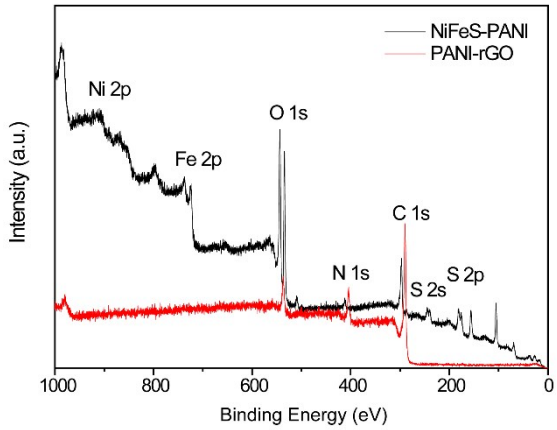

Figure S6. X-ray photoelectron spectroscopy (XPS) survey spectra of NiFeS-PANI and PANI-rGO. The N 1s spectrum in NiFeS-PANI is found to have a higher binding energy peak centered at a positive value compared to the neutral state N at 400 eV in emeraldine PANI. This high binding energy peak is partially attributed to the positively charged nitrogen.

	Atomic (%)					
	C 1s	N 1s	O 1s	S 2p	Fe 2p	Ni 2p
PANI-rGO	83.36	12.03	4.61	-	-	-
NiFeS-PANI	40.26	1.05	20.65	0.66	25.62	11.76

Table. Surface element composition of samples from XPS

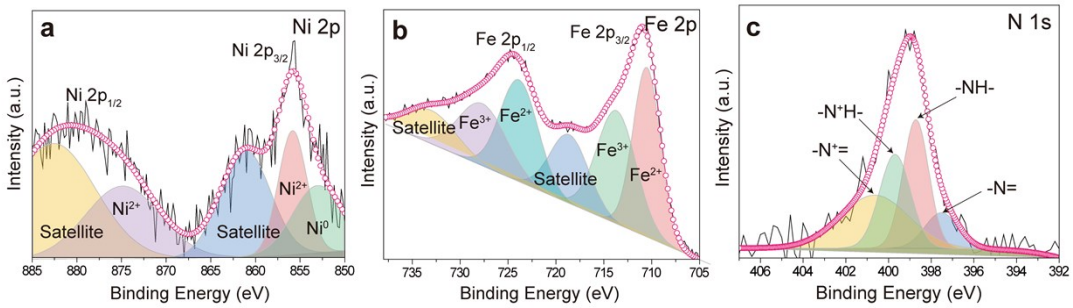

Figure S7. High-resolution XPS spectra of the (a) Ni 2p, (b) Fe 2p, and (c) N 1s for NiFeS-PANI after carbon (C 1s) calibration. The XPS peaks of N 1s are decomposed into three Gaussian peaks with binding energies of 397.5 (-N=), 398.7 (-NH-), 399.7 (-N^+-), and 400.6 (–N^+=). The peak at 400.6 eV and 399.7 eV are assigned to a quinoid amine and a benzenoid amine with nitrogen cationic radical (N^+), while the two peaks at 398.7 eV (-NH-) and 397.5 eV (=N–) are due to the quinoid amine and the benzenoid amine. The binding energy of the peak at 853 eV for the presence of NiS shows a sulfide species and corresponds to nickel disulfide. The nickel species present oxidation states of Ni^{2+} and Ni^0 at 855.8 eV and 853.0 eV, respectively. The Fe 2p spectrum featured a signal at 710.9 eV characteristic of the oxidation state of the nickel-iron sulfide composite, representing iron sulfide at 710.5 eV. Signals at 713.6 and 727.7 eV revealed that some of the iron atoms in this structure were in the Fe^{3+} oxidation state. The signals at 710.5 and 723.8 eV revealed that some of the iron atoms also existed as FeO in the Fe^{2+} oxidation state.

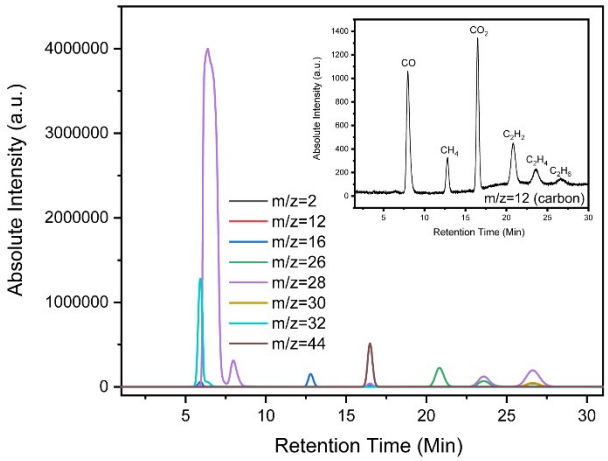

Figure S8. GC-MS control experiments using commercial calibration gas with defined fractions of C_1-C_2 products, and blank measurements with He.

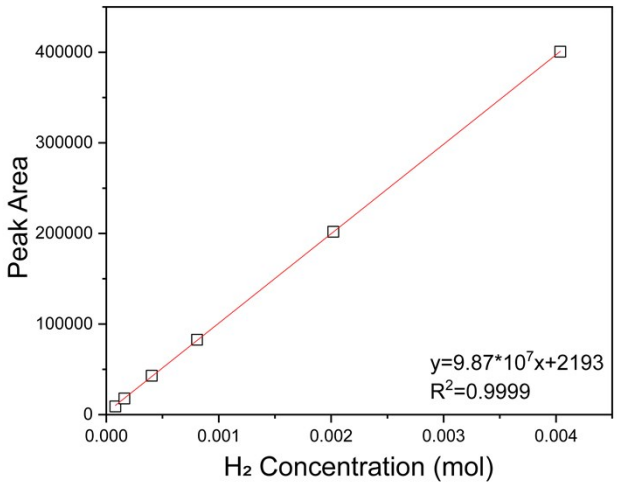

Figure S9. GC calibration curves for H_2 product using by TCD detector in Ar carrier gas. For analysis of unknown concentration samples, performing the same analysis on each concentration recognizes to plot a calibration curve from the average of the integrated spectra ($y=9.87810^7x+1345.02$ ($R^2=0.9999$)).

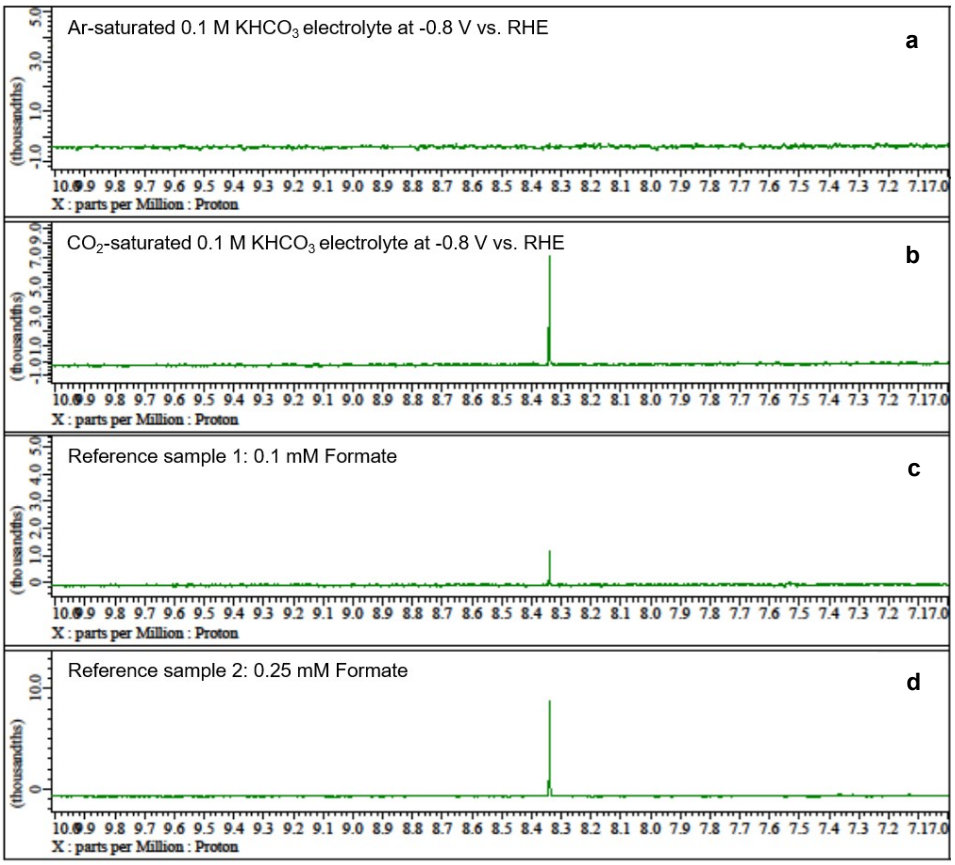

Figure S10. ^{1}H NMR analysis for NiFeS-PANI under (a) Ar- and (b) CO_2- saturated 0.1 M $KHCO_3$ at -0.8 V vs. RHE. (c) and (d) show ^{1}H NMR control experiments for reference concentration of formic acid.

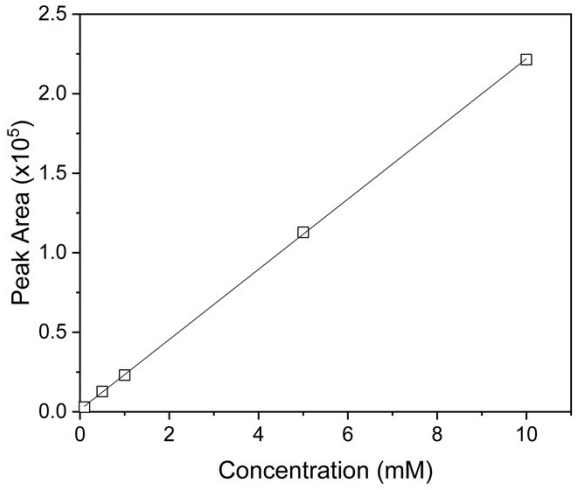

Figure S11. HPLC calibration curves for formic acid. For analysis of unknown concentration samples, performing the same analysis on each concentration recognizes to plot a calibration curve from the average of the integrated spectra (y=22063.7x+1345.02 (R^2=0.99994)).

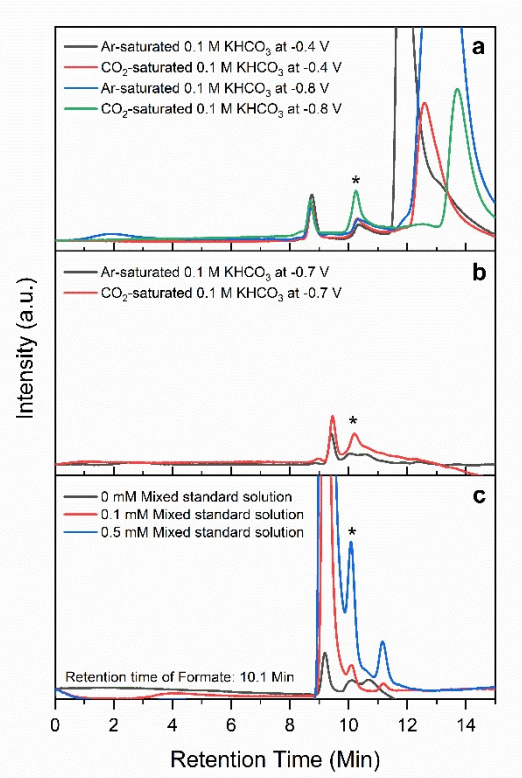

Figure S12. Detection of formic acid by HPLC analysis. The HPLC results of liquid products for (a) $FeNi_2S_4$ and (b) NiFeS-PANI nanostructures after 4 h of constant potential electrolysis at each potential (V vs. RHE) in Ar-saturated and CO_2-saturated 0.1 M $KHCO_3$ electrolyte. (c) the HPLC results of mixed standard solutions (pyruvate, formate, and acetate) in 0.1 M $KHCO_3$.

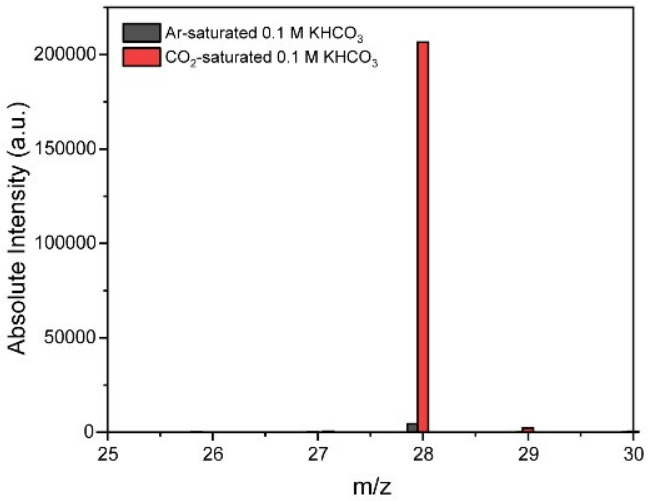

Figure S13. GC-MS analysis of NiFeS-PANI in Ar- and CO_2-saturated 0.1 M $KHCO_3$ electrolyte after 4 h of constant potential electrolysis at −0.7 V vs. RHE, showing the observed mass patterns of CO.

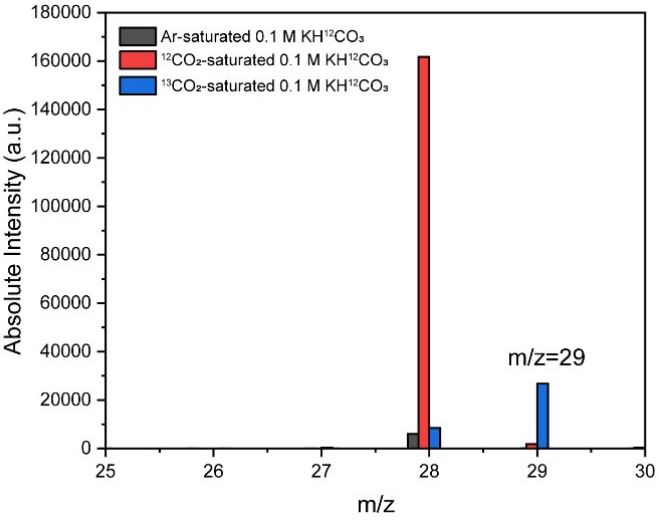

Figure S14. GC-MS analysis of $FeNi2S_4$ in Ar-, $^{12}CO_2$, $^{13}CO_2$-saturated 0.1 M $KH^{12}CO_3$ electrolyte after 4 h of constant potential electrolysis at −0.7 V vs. RHE, showing the observed mass patterns of CO. Before electrolysis using $^{13}CO_2$, the electrolyte was purged with Ar for 1 h to remove the dissolved CO_2; in a subsequent step, the electrolyte was purged with $^{12}CO_2$ and $^{13}CO_2$ for 1 h and 20 min, respectively.

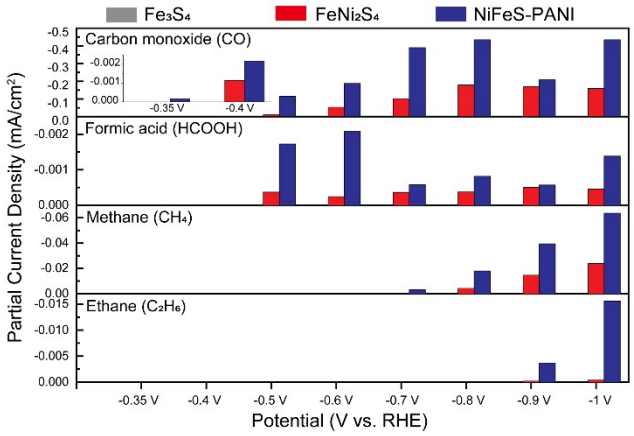

Figure S15. Partial current densities of CO_2 electroreduction products for Fe_3S_4, $FeNi_2S_4$, and NiFeS-PANI nanostructures after 4 h of constant potential electrolysis. Calculated partial current densities are shown for the detected products at each potential.

Figure S16. Comparison of partial current density of H_2, CO, CH_4, C_2H_6, and HCOOH for (a) NiFeS-PANI and (b) $FeNi_2S_4$.

Figure S17. Electrochemical double-layer capacitance for determining the electrochemically active surface area measurement. Cyclic voltammograms measured in a non-Faradaic region with scan rates of 10 to 400 mV s^{-1} for (a) $FeNi_2S_4$ and (b) NiFeS-PANI. (c) Capacitive current at 0.10 V (versus Ag/AgCl) as a function of scan rate for $FeNi_2S_4$ and NiFeS-PANI.

Geometric surface area of NiFeS-PANI and $FeNi_2S_4$

The electrochemical active surface area (ECSA) of the NiFeS-PANI and $FeNi_2S_4$ samples can be compared using electrochemical double-layer capacitance (C_{dl}) values. The C_{dl} values were determined by plotting the $j = j_a - j_c$ at the middle potential (0.1 V) against the CV scan rates for cyclic voltammetry curves obtained at non-faradaic potential regions (0.0–0.2 $V_{Ag/AgCl}$). The extracted slopes of the fitted lines allow comparison of the ECSA. As shown in Figure S7c, the C_{dl} values were obtained from the CV curves (Figure S6a and S6b). After determining the geometric surface areas for the NiFeS-PANI and $FeNi_2S_4$ samples, the partial current densities of all products were rationally calculated per the geometric surface area.

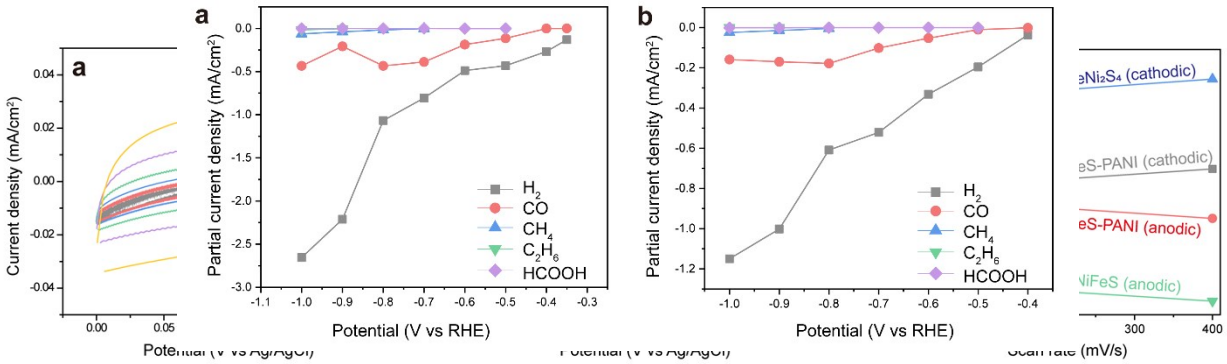

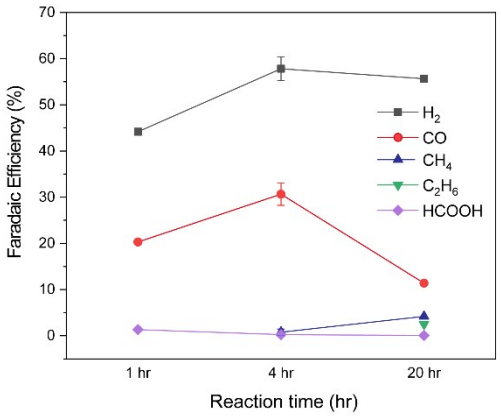

Figure S18. Analysis of CO_2 electroreduction products of NiFeS-PANI in CO_2-saturated 0.1 M $KHCO_3$ electrolyte at –0.7 V vs. RHE by chronoamperometry with a time-dependent analysis.

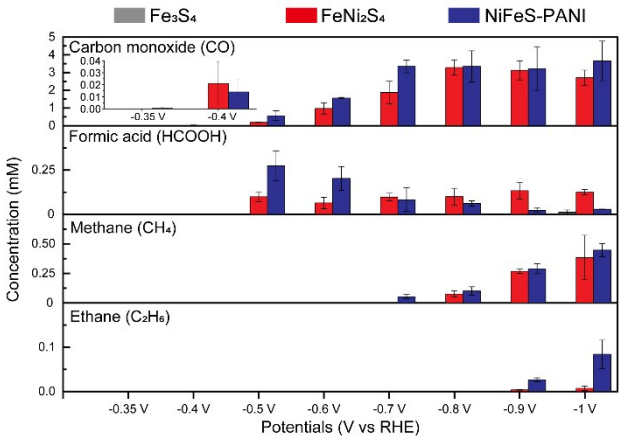

Figure S19. The concentration of all CO_2 electroreduction products for Fe_3S_4, $FeNi_2S_4$, and NiFeS-PANI nanostructures after 4 h of constant potential electrolysis.

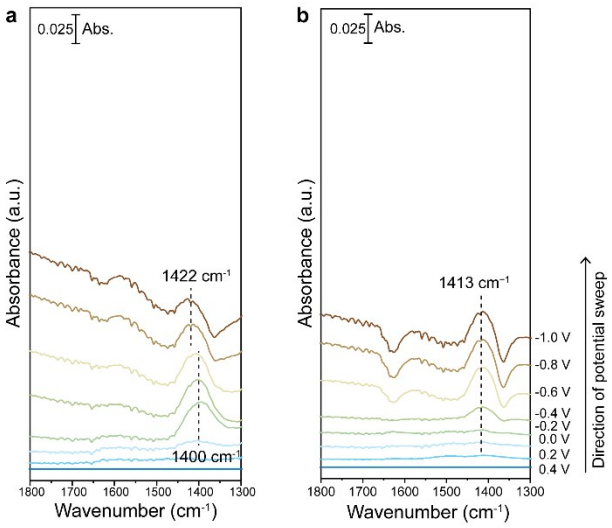

Figure S20. *In situ* ATR-FTIR spectra of (a) $FeNi_2S_4$ and (b) NiFeS-PANI nanostructures in Ar-saturated 0.1 M $KDCO_3$ electrolyte. The spectra collected at +0.4 V vs. RHE were used as the reference.

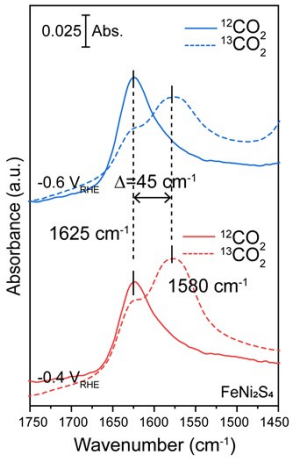

Figure S21. *In situ* ATR-FTIR spectra of $FeNi_2S_4$. An isotope shift of the species with ^{13}C-labeled CO_2 at 1625 cm^{-1} was observed on $FeNi_2S_4$ at −0.4 and −0.6 V vs. RHE.

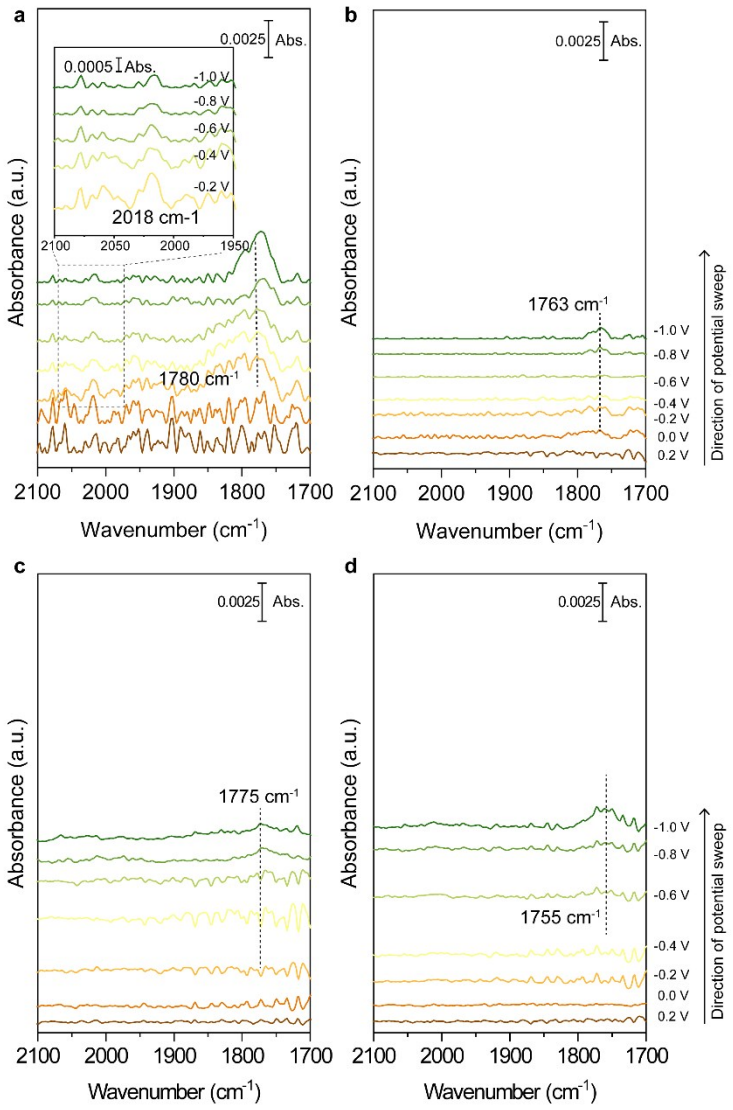

Figure S22. *In situ* ATR-FTIR spectra recorded for (a) $FeNi_2S_4$ and (c) NiFeS-PANI nanostructures in CO_2-0.1 M $KDCO_3$ electrolyte with the 1650-1850 cm^{-1} region. Spectra showing the isotope shift in $^{13}CO_2$-saturated 0.1 M $KDCO_3$ electrolyte on (b) $FeNi_2S_4$ and (d) NiFe-PANI. The spectra collected at +0.4 V vs. RHE were used as the reference.

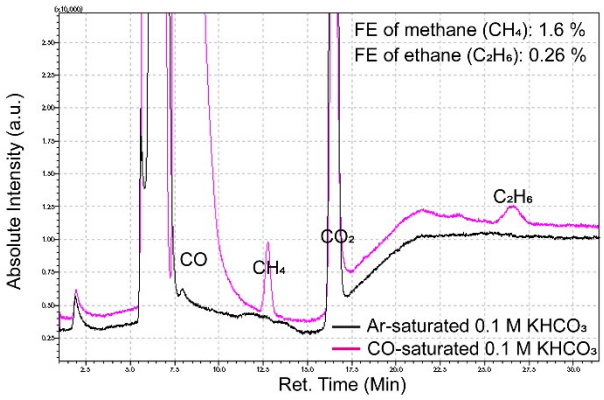

Figure S23. Electrochemical reduction of CO by $FeNi_2S_4$. GC results after bulk electrolysis at -0.8 V vs. RHE for 3.5 h in CO-saturated 0.1 M $KHCO_3$ electrolyte.